

Aspects of 3-D Imaging by Classical Tomography for Dual Detector PEM

M. F. Smith¹, S. Majewski¹, A. G. Weisenberger¹, D. Kieper¹, J. D. Kalen², P. P. Fatouros²

¹Thomas Jefferson National Accelerator Facility, Newport News, VA 23606

²Department of Radiology, Virginia Commonwealth University Health System, Richmond, VA 23298

ABSTRACT

Images from dual detector positron emission mammography (PEM) systems are commonly reconstructed by backprojection methods of classical tomography. Characteristics of 3-D PEM images were investigated using analytic models and computer simulations, in particular depth resolution and the quality of images in the third dimension normal to the detectors. These modeling tools provide insight into the depth blurring observed in 3-D images from experimental line source and breast phantom studies acquired with detectors built using pixellated arrays of LGSO crystals. Approaches to improved 3-D breast imaging are discussed.

I. INTRODUCTION

Positron emission mammography (PEM) with F-18 fluorodeoxyglucose (FDG) has the capability to image regions of increased metabolic activity in the breast, which may prove useful in the detection, staging and treatment of breast cancer. Several groups, including our own, have built or are developing dedicated PEM imaging systems. System designs include parallel planar detectors [1-3], curved plate detectors [4] and small ring configurations [5, 6]. Clinical breast imaging with FDG is an area of active research [7-9].

With dual detector PEM the breast is imaged between two static parallel planar detectors. There is incomplete angular sampling in planes perpendicular to the detectors. Image reconstruction is commonly performed in planes parallel to the detectors using the backprojection method of classical tomography [10]. In a simulation study 2-D iterative reconstruction in perpendicular planes was implemented after single slice rebinning [5]. For both methods there is blurring between the detectors due to incomplete angular sampling.

The goal of this work is to provide a better understanding of some aspects of classical tomography reconstruction performance for 3-D PEM image formation. In particular, depth resolution and the quality of images normal to the detectors will be investigated. Analytic and computer modeling will be used and results from physical experiments will be presented.

II. ANALYTIC MODEL

In this section a model of the angle-dependent point source sensitivity will be used to estimate the intensity of a point source in different reconstructed image planes. These values will be used to estimate resolution normal to the detectors.

A. Point Source Sensitivity

Consider a simple PEM detector model where the two planar detector heads are parallel and separated by a distance D (Figure 1). Assume that each detector has an efficiency s for

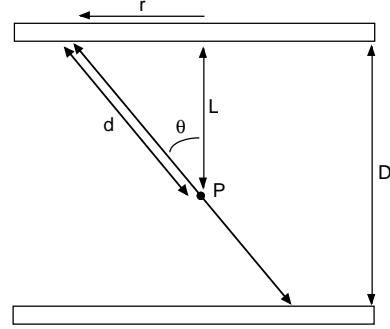


Figure 1. Diagram of the geometry of the point source between the two PEM detectors.

detection of an annihilation photon and that photons are detected at the front surface of the detectors.

Now suppose that a point source of activity A (positron emissions/sec) is located at position P that is a distance L from one of the detector heads. The photon flux density from annihilation photons (counts/sec/unit area) on the surface of that detector is

$$f(r) = (A / (2\pi d^2)) \cos \theta = (A / 2\pi) (L / (L^2 + r^2)^{3/2}) \quad (1)$$

where r is the distance from the orthogonal projection of point P onto the detector surface and θ is the angle from normal incidence. Equation (1) can be integrated for the photon flux within an acceptance angle θ_{\max} from normal incidence,

$$F(\theta_{\max}) = A(1 - \cos \theta_{\max}) \quad (2)$$

The total flux will be the same on the opposing detector.

The geometric efficiency for detection of annihilation events is $1 - \cos \theta_{\max}$ and the total sensitivity is $s^2 (1 - \cos \theta_{\max})$. Use of a larger acceptance angle in image reconstruction will increase sensitivity, which should decrease statistical noise in the resulting images and enable better detection of smaller and lower contrast tumors. Increasing the acceptance angle will degrade image uniformity, however [3].

B. Depth Resolution for an Ideal Detector and Circular Pixels

Reconstructed images are formed in planes parallel to the detectors by backprojecting counts along the lines of response connecting the detection locations of the annihilation photons. The resulting images are the sum of a focused image of activity in the desired plane and blurred images of activity in other planes. The point spread function normal to the detectors can be derived for the case of an ideal detector with infinitely small pixels and backprojection into circular image pixels.

In the image plane containing the point source, all events within the axial acceptance angle will contribute to the pixel

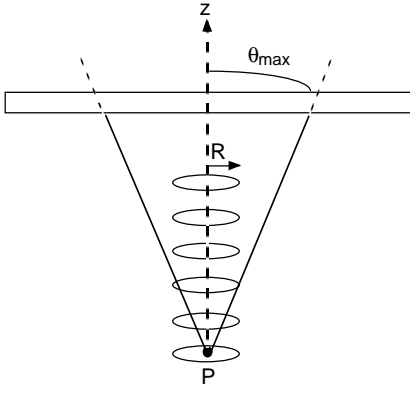


Figure 2. Diagram of circular pixels of radius R in different image planes.

containing the source point (Figure 2). Now consider a circular pixel of radius R that is located a distance z from the point source along a line perpendicular to the detector face. The maximum angle from the normal of annihilation photons originating at point P that pass through this circle is $\theta_z = \arctan(R/z)$. If the maximum acceptance angle for image reconstruction is θ_{\max} , then the photon flux from point P contributing to reconstructed counts in this pixel is

$$F(\theta_z) = A (1 - \cos(\min\{\theta_z, \theta_{\max}\})) \quad (3)$$

The normalized point spread function (PSF) perpendicular to the detector follows from equations (2) and (3) as

$$\begin{aligned} PSF(z) &= (1 - \cos(\min\{\theta_z, \theta_{\max}\})) / (1 - \cos \theta_{\max}) \\ &= \min\{(1 - 1/[1 + (R/z)^2]^{1/2}) / (1 - \cos \theta_{\max}), 1\} \end{aligned} \quad (4)$$

A measure of the imaging resolution perpendicular to the detector face is given by the full-width at half-maximum (FWHM) of the PSF. From equation (4) this is

$$FWHM(\theta_{\max}) = R(1 + \cos \theta_{\max}) / [1 - (1/4)(1 + \cos \theta_{\max})^2]^{1/2} \quad (5)$$

For the discrete case where the image of a point source is reconstructed into square pixels that are the same size as the detector pixels, the image counts are usually spread among a few pixels in the focal plane. The maximum pixel value is a factor $\beta < 1$ times the total image counts and is dependent on the location of the point source with respect to the discretization grid. For this more general case an expression for the PSF normal to the detectors has not yet been derived, however we have found empirically that the FWHM of small point sources often can be modeled by

$$FWHM(\theta_{\max}) = 2R[1 - (\beta/2)(1 - \cos \theta_{\max})] / \{1 - [1 - (\beta/2)(1 - \cos \theta_{\max})]^2\}^{1/2} \quad (6)$$

which reduces to equation (5) when $\beta=1$.

As an example, consider the case of circular pixels 3.39 mm in diameter (area 9 mm²). The dependence of the PSFs on maximum acceptance angle is shown in Figure 3. The resolution normal to the detectors improves when the

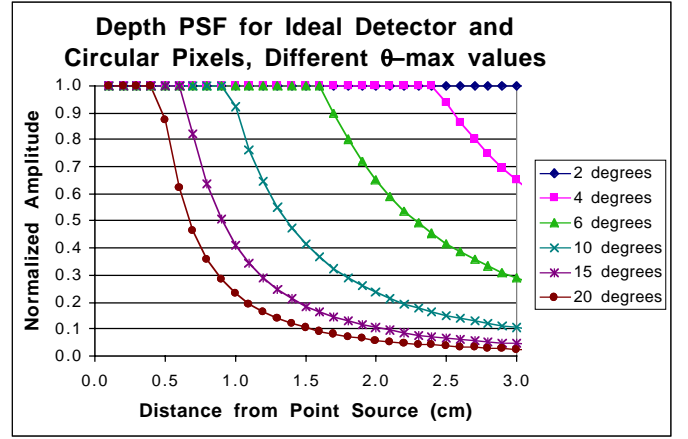


Figure 3. Point spread functions normal to the detector for different maximum acceptance angles (θ_{\max}) of coincidence events (equation (4)). An ideal detector is modeled and the circular image pixels are 3.4 mm in diameter.

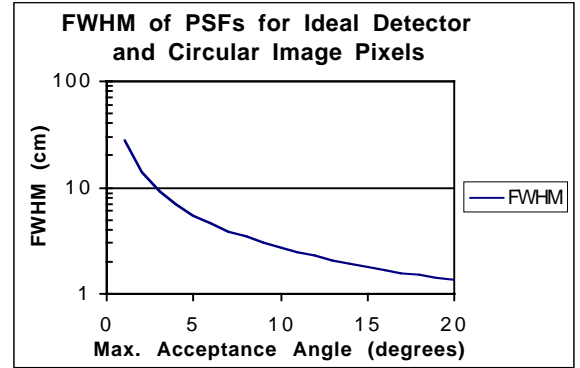


Figure 4. Full-width at half-maximum of the PSFs normal to the detector as a function of the maximum acceptance angle of coincidence events contributing to the backprojection images (equation (5)). An ideal detector is modeled and the circular image pixels are 3.4 mm in diameter.

acceptance angle increases because the point sources are increasingly blurred in non-focal planes (Figure 4).

III. NUMERICAL SIMULATIONS AND PHYSICAL EXPERIMENTS

A. Point Source

Point source acquisitions were simulated for a PEM system with pixellated detectors. The computer program for these simulations employed ray-tracing and numerical integration methods. Photons were assumed to be detected at the surface of the detectors. The detector heads were modeled as 29 x 29 arrays of 3.3 mm pixels, the same geometry as PEM detectors we have built [3]. The detector separation was 18 cm.

Image reconstruction was by classical tomography with a pixel size of 3.3 mm and image plane spacing of 3.3 mm. Images were reconstructed with acceptance angles of 5, 10, 15 and 20 degrees. Depth resolution improves with increasing acceptance angle, though there is considerable blurring in the images (Figure 5) and in vertical profiles through the point sources (Figure 6). The FWHM of the profiles are 10.6, 5.2, 3.6 and 2.7 cm for 5, 10, 15 and 20 degree acceptance angles,

respectively. The widths predicted by equation (6) with $\beta = 0.29$ are 11.2, 5.6, 3.7 and 2.8 cm, respectively.

B. Line Source

Coincidence data were acquired with a PEM system built with a pixellated detector array of LGSO crystals (Hitachi, Inc.). Each detector head was 10 cm x 10 cm with a 29 x 29 crystal array; the individual crystals were 3 mm x 3 mm x 10 mm and the crystal pitch was 3.3 mm. The crystals were coupled to an array of 4 x 4 Hamamatsu R7600-00-C8 position sensitive photomultiplier tubes. The rest of the detector design has been described elsewhere [3].

Three line sources were filled with F-18 and placed midway between the detector heads, which were separated by 18 cm. Images were reconstructed in the central 21 slices with a spacing of 3.3 mm using 10 and 20 degree acceptance angles. Blurring normal to the detectors is more severe for the smaller acceptance angle (Figure 7). Depth resolution differs for the line sources because of the more limited angular range of lines of response near the edge of the detector.

C. Breast Phantom with Tumors

A 6 cm thick box phantom simulating a compressed breast was filled with 33 nCi/cc F-18 and imaged for 10 min with the previously described PEM system. The distance between the detector heads was 7.5 cm. Simulated tumors 12 mm, 10 mm, 8 mm and 4 mm diameter were filled with activity in a 10:1 tumor:background activity concentration ratio. Images were reconstructed for 21 slices with a 3.3 mm spacing using a coincidence acceptance angle of 20 degrees. The three larger tumors are visible in their focal plane, but there is appreciable blurring normal to the detectors (Figure 8).

IV. DISCUSSION

The analyses and simulations of this paper were simple ones and they represent an initial effort toward quantifying depth-dependent blurring for PEM. This is an important issue since classical tomography is widely used for dual detector PEM image reconstruction. Depth-dependent blurring as well as sensitivity, image uniformity and image noise are all affected by the maximum acceptance angle chosen for reconstruction.

The analytic expression for the PSF normal to the detector could be improved by generalizing it to model discretization of the detectors and of the backprojected images. The computer simulations of the PEM system could be made more realistic by better modeling photon interactions in the source region and detector.

Image reconstruction by classical tomography has advantages and disadvantages for dual detector PEM. One advantage is high sensitivity since all of the coincidence data within a given acceptance angle can be used in image reconstruction, reducing statistical noise. It is fast enough that image reconstruction can be implemented in real-time as part of data acquisition [2].

The major disadvantage of classical tomography is that activity from neighboring planes is blurred into the image

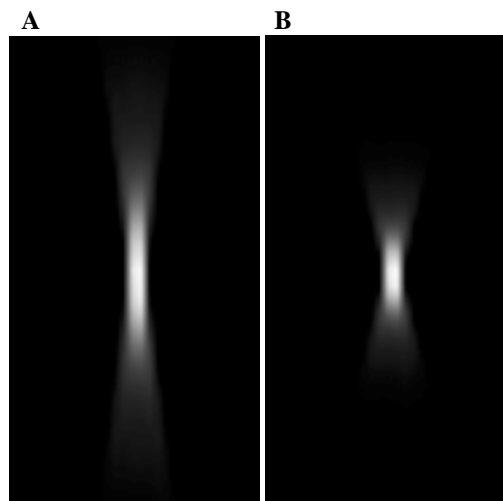


Figure 5. Images normal to the detector face of reconstructions of a point source for (a) 10 degree and (b) 20 degree acceptance angles. The detectors would be positioned at the top and bottom of each image.

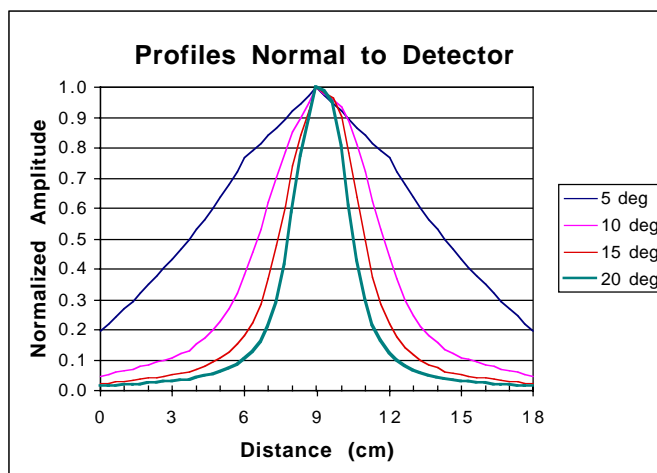


Figure 6. Profiles normal to the detectors for a point source simulation and image reconstruction with different acceptance angles. The images corresponding to the 10 and 20 degree curves are shown in Figure 5.

plane, not removed as for computed tomography. It would be interesting to investigate whether low contrast lesions can be detected or localized better in classical tomography images or in limited angle computed tomography images reconstructed from the same dataset, particularly for compressed breasts. A broader question is whether there are better methods for extracting 3-D information from coincidence data acquired with dual detector PEM.

A more general challenge for PEM is the optimization of detector design (e.g. planar detectors, curved detectors, ring detectors), detector motion (static, few or many detector positions), image reconstruction method (classical tomography, computed tomography, iterative reconstruction), breast positioning (uncompressed vs. compressed) and other factors for the desired detection or quantitation task.

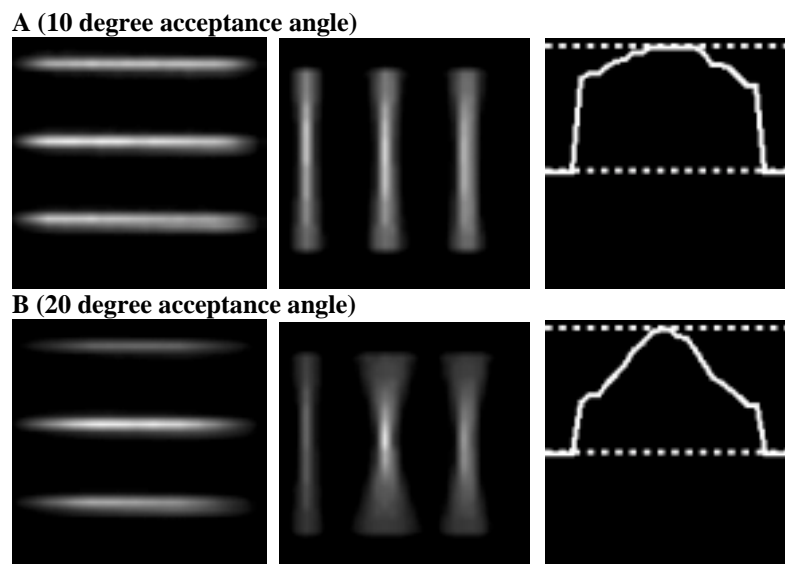


Figure 7. Images of line sources from an experimental acquisition for (a) 10 degree and (b) 20 degree acceptance angles. (left) Focal plane image parallel to the detectors, (center) image normal to the detectors and (right) vertical profile through the center line source of the image normal to the detectors. Only the center 21 slices spaced at 3.3 mm were reconstructed.

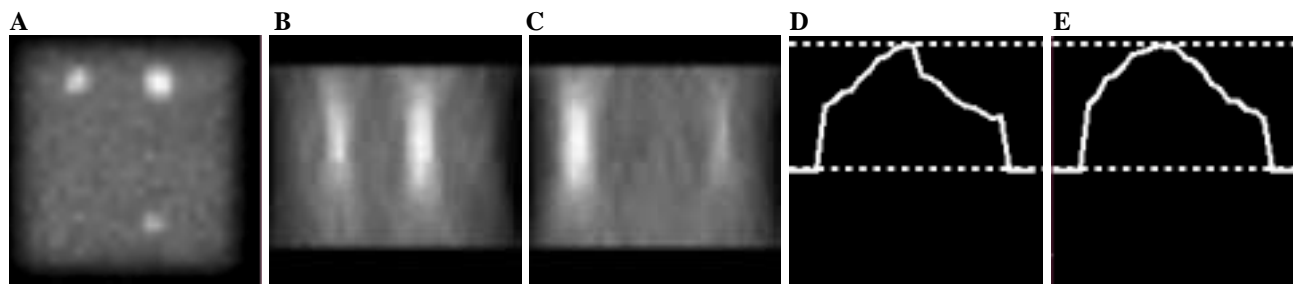


Figure 8. Images of a compressed breast phantom with simulated tumors from an experimental acquisition. Image reconstruction was with a 20 degree acceptance angle. (a) Focal plane image parallel to the detectors, (b) image normal to the detectors through the upper two tumors of (a), (c) image normal to the detectors through the tumors on the right side of (a), (d) vertical profile through the left tumor of (b), (e) vertical profile through the right tumor of (b).

V. CONCLUSION

Three-dimensional imaging for a dual detector positron emission mammography system has been investigated for image reconstruction by classical tomography. Analytic models and computer simulations of a PEM system provide insight into the blurring normal to the detectors observed in reconstructed PEM images from experimental line source and breast phantom acquisitions. Improved methods of extracting 3-D information from PEM coincidence data would be beneficial.

VI. REFERENCES

- [1]C. J. Thompson, K. Murthy, Y. Picard, I. N. Weinberg, and R. Mako, "Positron emission mammography (PEM): a promising technique for detecting breast cancer," *IEEE Trans. Nucl. Sci.*, vol. 42, pp. 1012-1017, 1995.
- [2]I. N. Weinberg, S. Majewski, A. G. Weisenberger, A. Markowitz, L. Aloj, L. Majewski, D. Danforth, J. Mulshine, K. Cowan, J. Zujewski, C. Chow, E. Jones, V. Chang, W. Berg, and J. Frank, "Preliminary results for positron emission mammography: real-time functional breast imaging in a conventional mammographic gantry," *Eur. J. Nucl. Med.*, vol. 23, pp. 804-806, 1996.
- [3]R. R. Raylman, S. Majewski, R. Wojcik, A. G. Weisenberger, B. Kross, V. Popov, and H. A. Bishop, "The potential role of positron emission mammography for detection of breast cancer. A phantom study," *Med. Phys.*, vol. 27, pp. 1943-1954, 2000.
- [4]R. Freifelder, J. S. Karp, S. Surti, and J. A. Wear, "A dedicated PET scanner for breast imaging using two curve-plate NaI(Tl) detectors," *J. Nucl. Med.*, vol. 39, p. 171P, 1998.
- [5]R. Freifelder and J. S. Karp, "Dedicated PET scanners for breast imaging," *Phys. Med. Biol.*, vol. 42, pp. 2463-2480, 1997.
- [6]H. Baghaei, W.-H. Wong, J. Uribe, H. Li, N. Zhang, and Y. Wang, "Breast cancer imaging studies with a variable field of view PET camera," *IEEE Trans. Nucl. Sci.*, vol. 47, pp. 1080-1084, 2000.
- [7]R. L. Wahl, M. A. Helvie, A. E. Chang, and I. Andersson, "Detection of breast cancer in women after augmentation mammoplasty using fluorine-18-fluorodeoxyglucose-PET," *J. Nucl. Med.*, vol. 35, pp. 872-875, 1994.
- [8]K. Yutani, M. Tatsumi, E. Shiba, H. Kusuoka, and T. Nishimura, "Comparison of dual-head coincidence gamma camera FDG imaging with FDG PET in detection of breast cancer and axillary lymph node metastasis," *J. Nucl. Med.*, vol. 40, pp. 1003-1008, 1999.
- [9]K. Murthy, M. Aznar, C. J. Thompson, A. Loutfi, R. Lisbona, and J. H. Gagnon, "Results of preliminary clinical trials of the positron emission mammography system PEM-I: a dedicated breast imaging system producing glucose metabolic images using FDG," *J. Nucl. Med.*, vol. 41, pp. 1851-1858, 2000.
- [10]H. H. Barrett and W. Swindell, *Radiological Imaging: The Theory of Image Formation, Detection and Processing*. New York: Academic, 1981.